Supporting Information

A Pompon-Like RuNPs-Based Theranostic Nanocarrier System with Stable Photoacoustic Imaging Characteristic for Accurate Tumor Detection and Efficient Phototherapy Guidance

Gengjia Chen[a, †], Meng Xu [a, †], Shuang Zhao[a], Jing Sun[a], Qianqian Yu[a], Jie Liu*[, a]
[a] Department of Chemistry, Jinan University, Guangzhou 510632, China
* Corresponding author. Tel: +86 20 85220223. Fax: +86 20 85220223. E-mail: tliuliu@jnu.edu.cn.
[†] These authors contributed equally to the work.

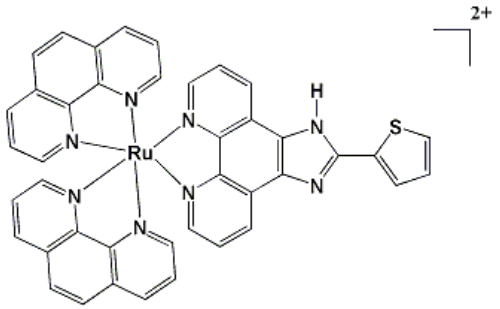

Figure S1. Schematic structures of $[Ru(bpy)2(tip)]^{2+}$.

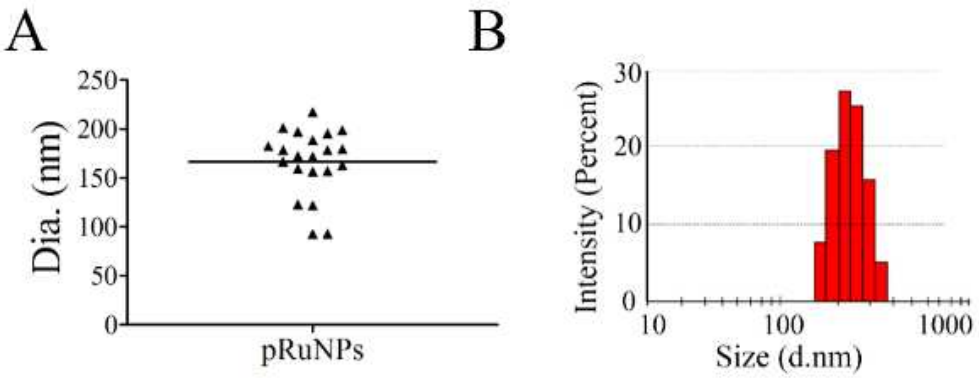

Figure S2. A) The quantitative analysis of the diameter of pRuNPs based on Figure 1A. B) Size distribution of pRuNPs determined by dynamic light scattering (DLS).

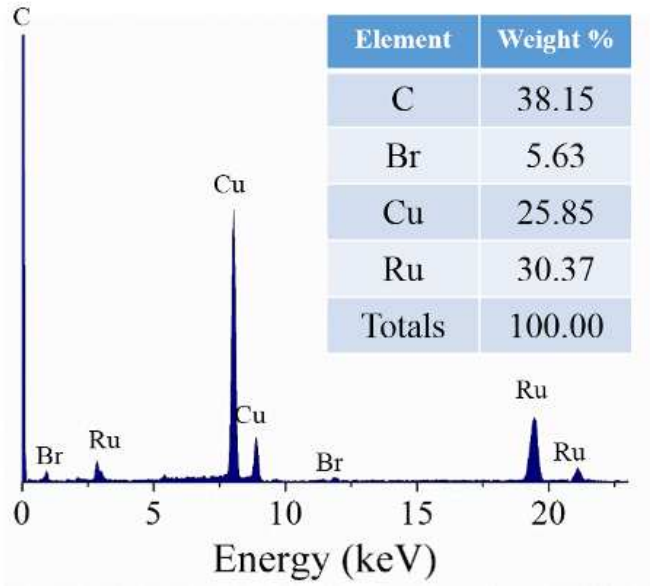

Element	Weight %
C	38.15
Br	5.63
Cu	25.85
Ru	30.37
Totals	100.00

Figure S3. Elemental analysis of pRuNPs by energy-dispersive X-ray (EDX) spectrum.

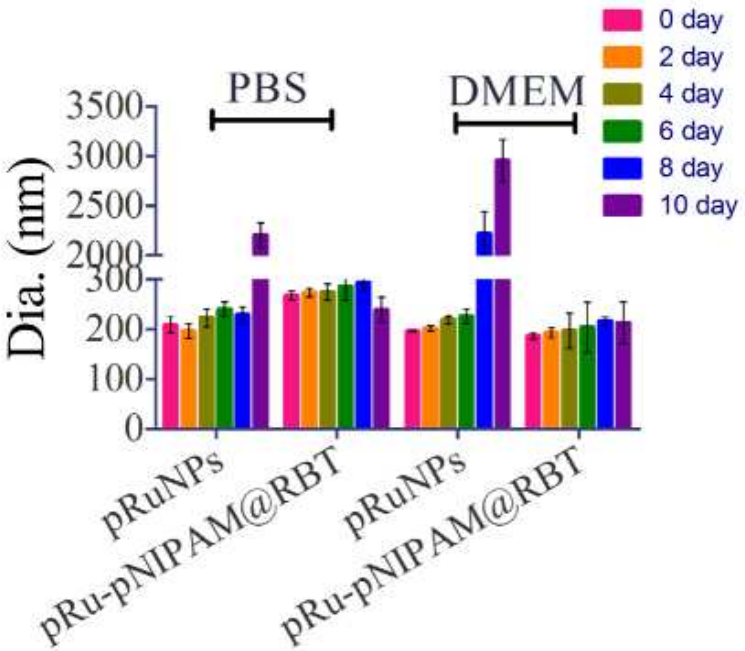

Figure S4. Size variations of pRuNPs and pRu-pNIPAM@RBT in PBS or DMEM for 10 days.

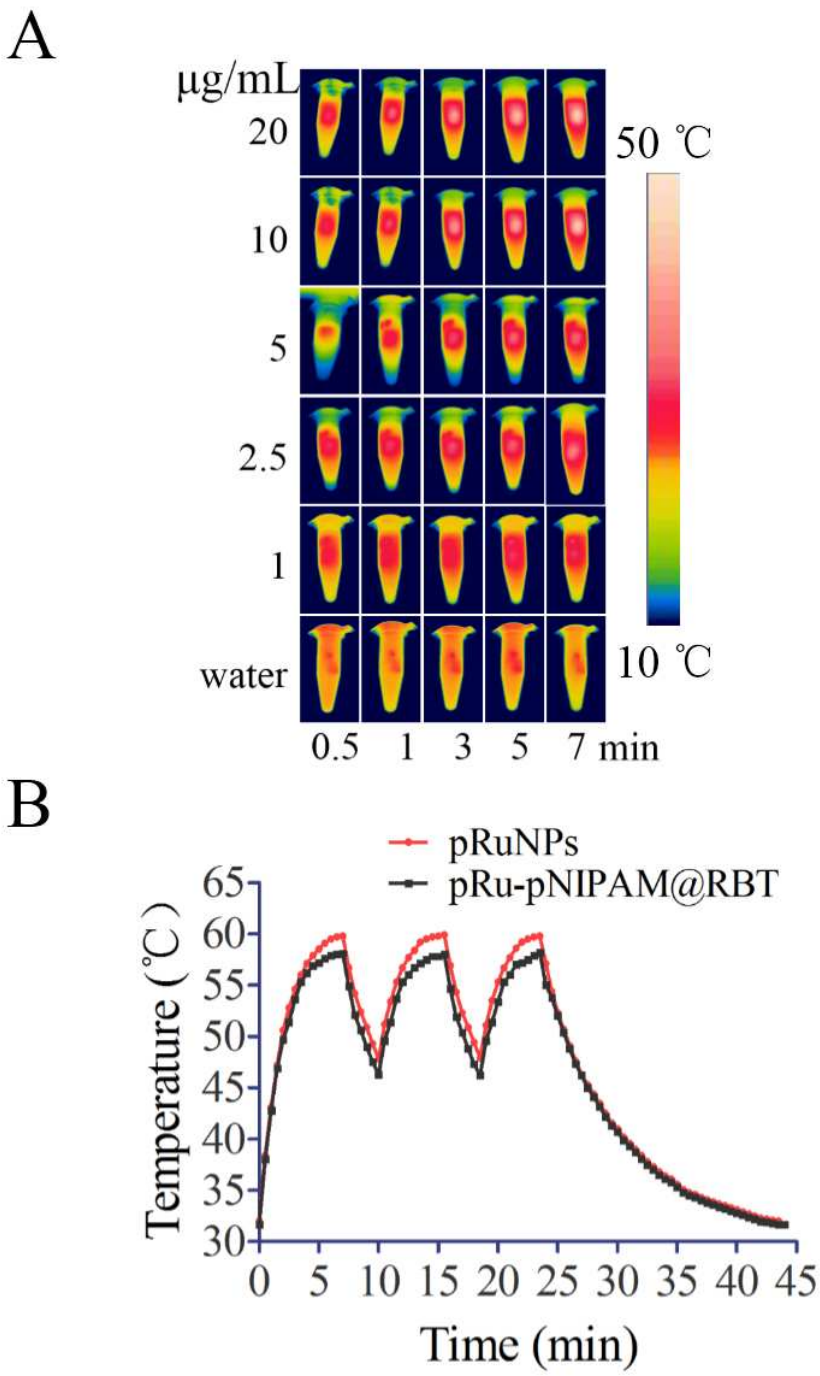

Figure S5. (A) IR thermal image of various concentrations of pRu-pNIPAM@RBT under 808 nm laser irradiation for 7 min. (B) The corresponding temperature-time curve of pRuNPs and pRu-pNIPAM@RBT during the continuous three-time heating-cooling cycles.

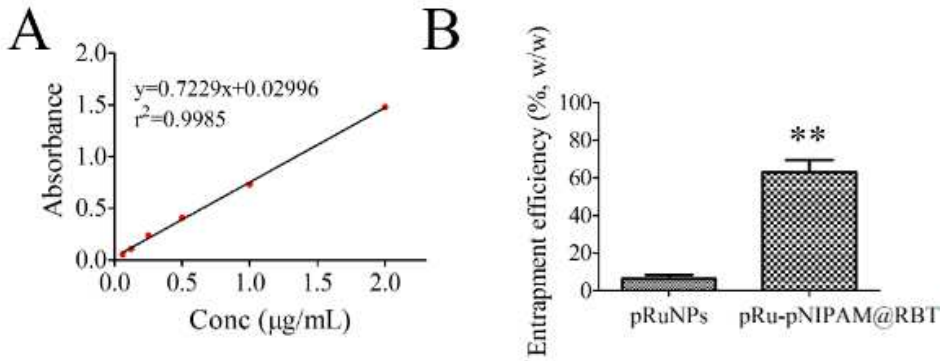

Figure S6. A) Corresponding linear fit between concentration of RBT and absorbance as detected by UV-vis spectra. B) Entrapment efficiency of RBT in pRuNPs and pRu-pNIPAM@RBT, respectively. **P<0.01, significant difference between pRuNPs and pRu-pNIPAM@RBT group. The error bars represent the standard error of mean (n = 5).

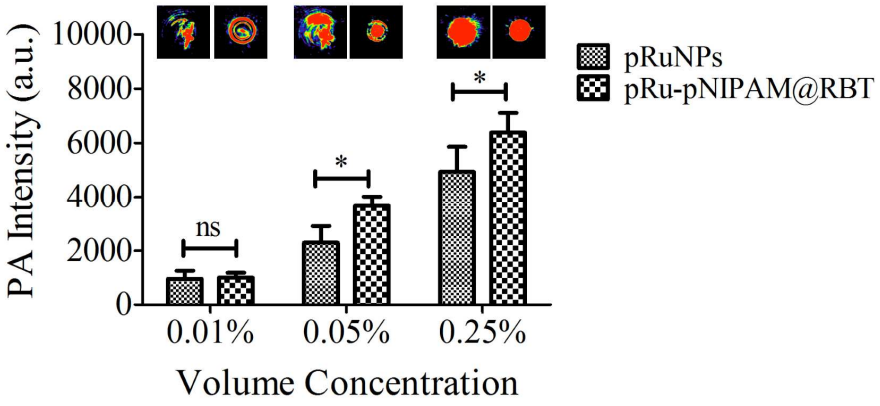

Figure S7. PA signal intensity of pRuNPs and pRu-pNIPAM@RBT at various volume concentrations. *P<0.05, the error bars represent the standard error of mean (n = 3).

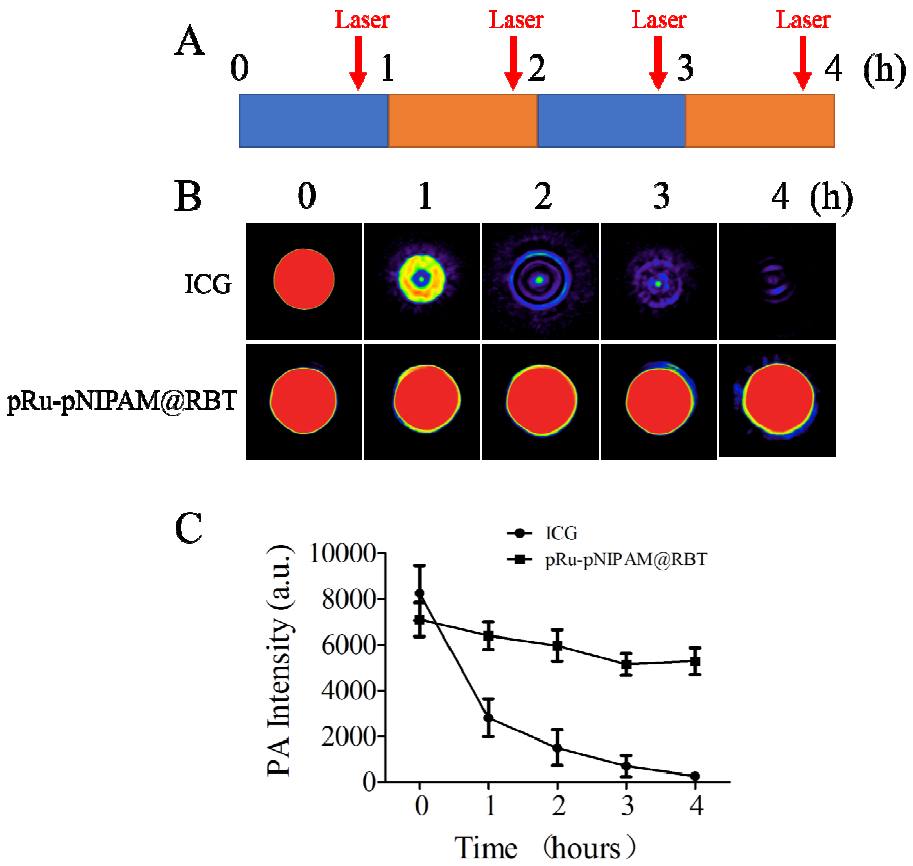

Figure S8. A) Schematic diagram of irradiation schedule of ICG and pRu-pNIPAM@RBT, for one minute each time. (1.0 W/cm2). B) PA imaging of ICG and pRu-pNIPAM@RBT at indicated time. C) Quantitative analysis of PA signal intensities obtained with ICG and pRu-pNIPAM@RBT.

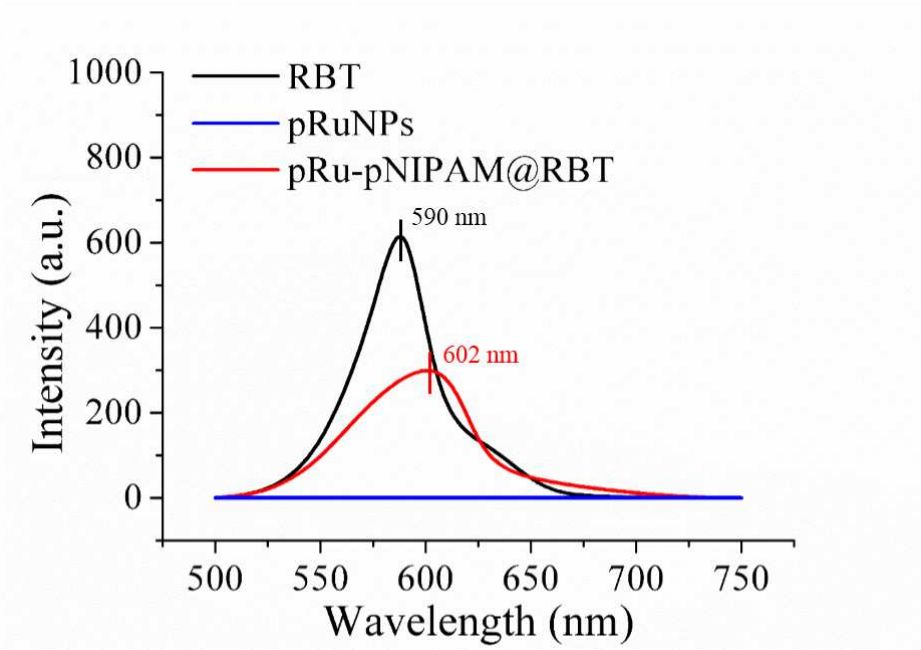

Figure S9. Fluorescence spectra of RBT, pRuNPs and pRu-pNIPAM@RBT acquired in aqueous solution, excitation wavelength 460 nm.

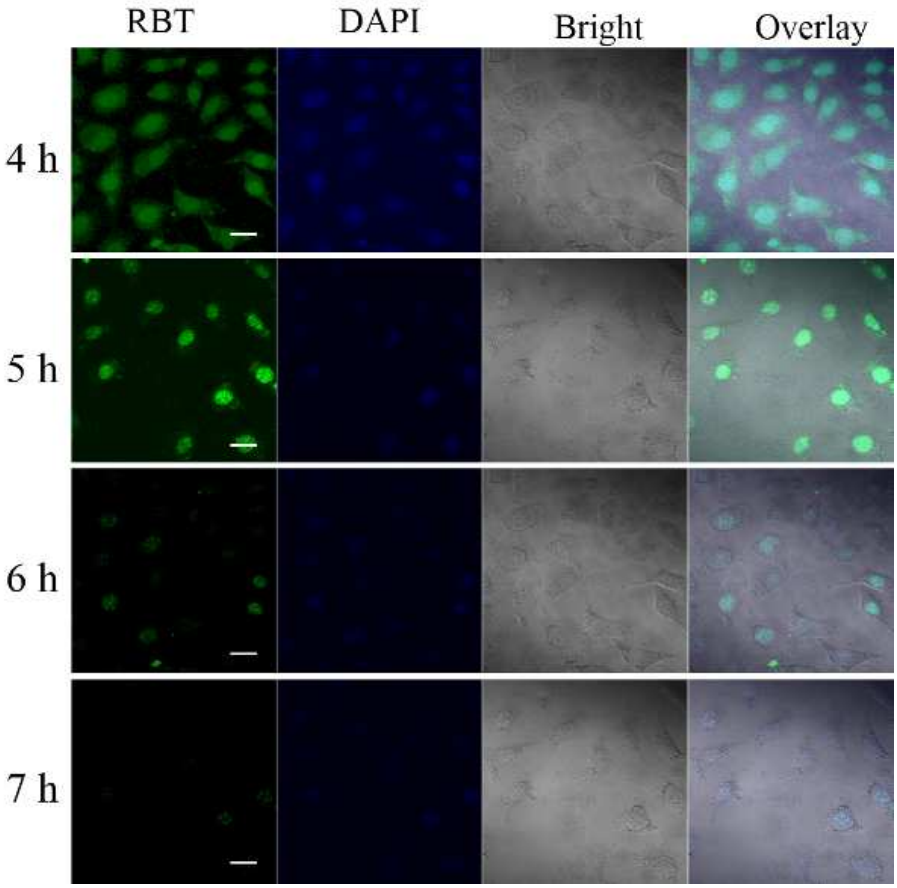

Figure S10. Localization of free RBT (green) and nuclei labeled by DAPI (blue). Scale bar: 25 μm.

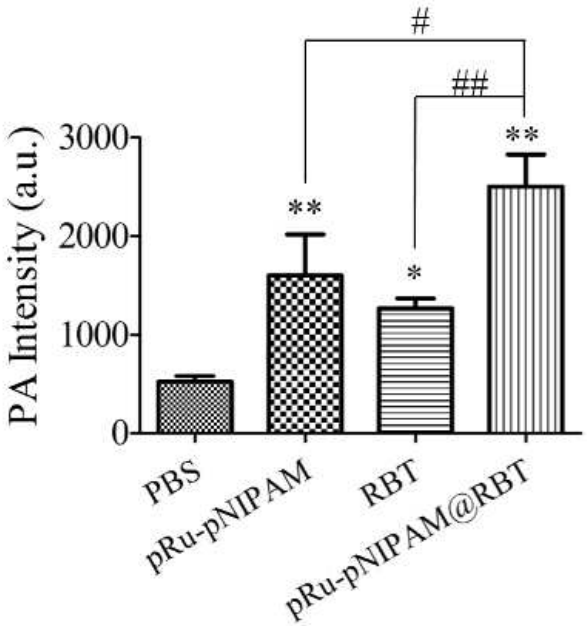

Figure S11. Quantitative analysis of the PA intensity of tumors based on Figure 8A. *P<0.05, **P<0.01, significant difference compared to PBS group; #P<0.05, ##P<0.01, significant difference compared to pRu-pNIPAM@RBT group. The error bars represent the standard error of mean (n = 5).

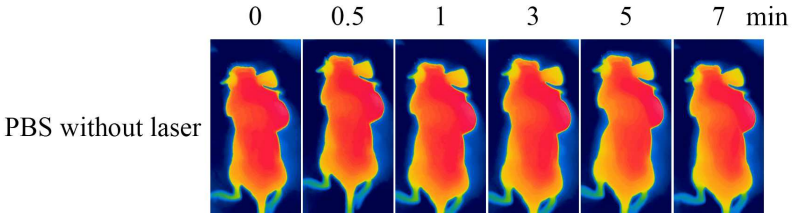

Figure S12. IR thermal image of tumor-bearing nude mouse after intratumorally injecting with PBS without laser irradiation.

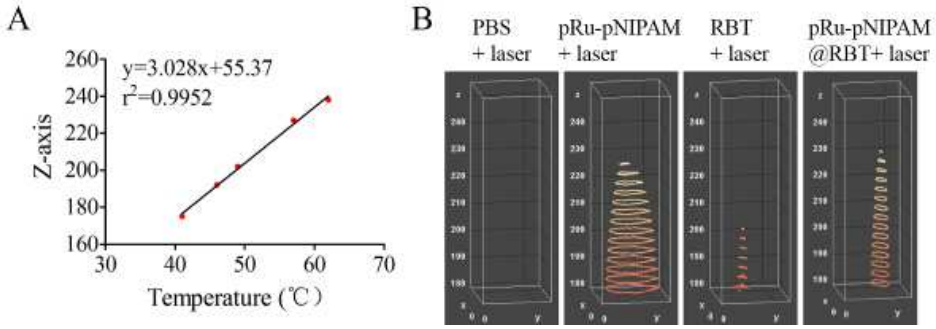

Figure S13. A) Corresponding linear fit between temperature and Z-axis based on Figure 9B. B) The 3D temperature distribution images above 42°C.

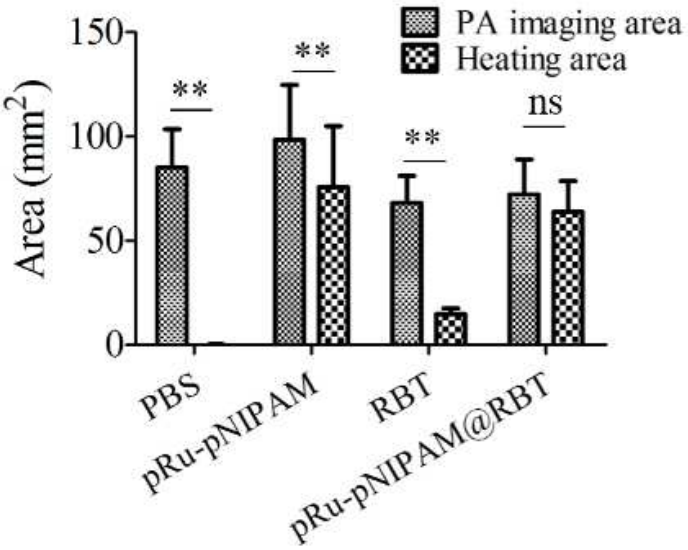

Figure S14. Comparison between the cross-sectional area of tumor and effective area of phototherapy based on Figure 8A and Figure 9C. **P<0.01, significant difference between PA imaging area and heating area group; ns = not significant. The error bars represent the standard error of mean (n = 5).

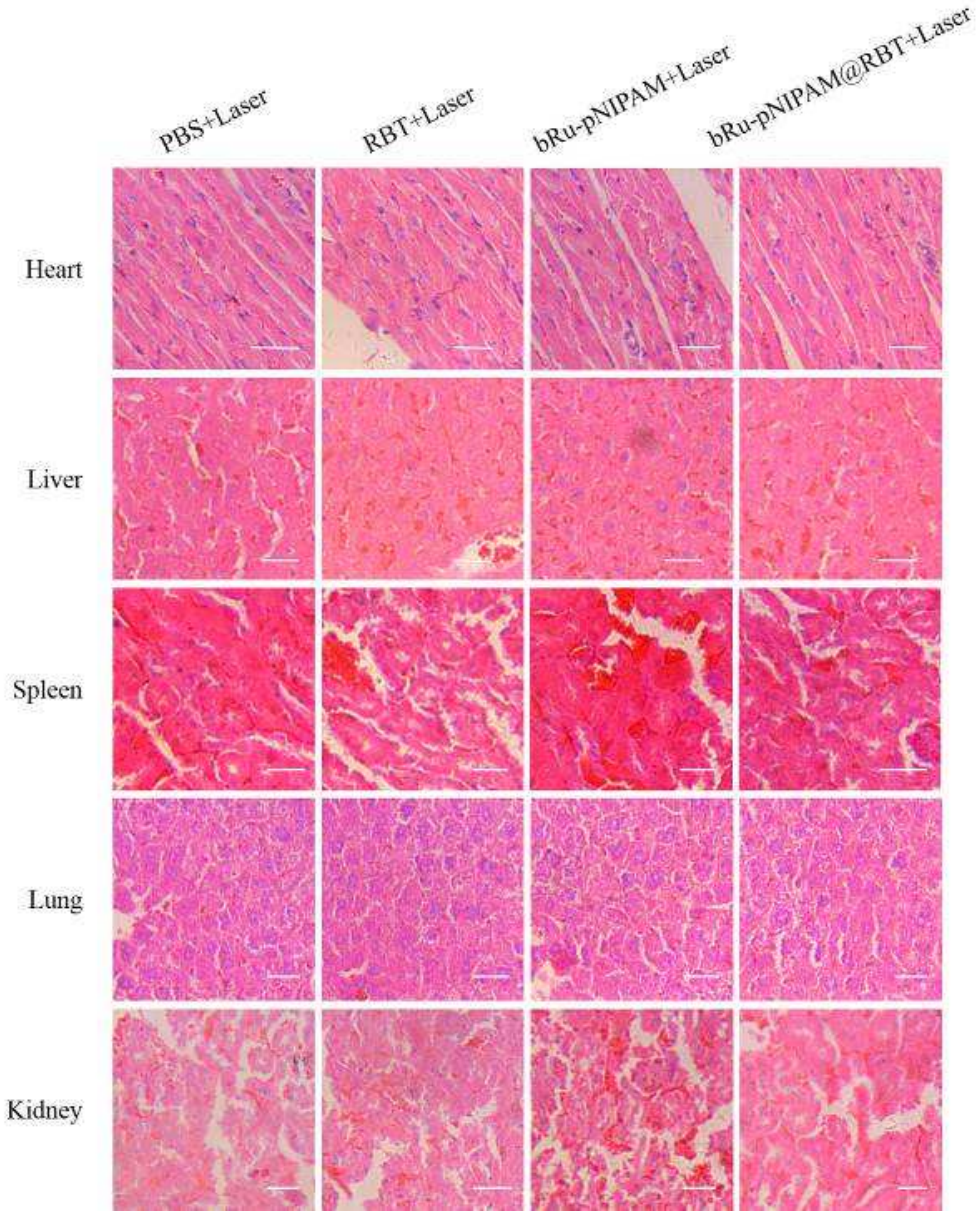

Figure S15. H&E images of major organs (heart, liver, spleen, lung and kidney) collected from HepG2 tumor bearing mice after different treatments for 15 days. Scare bar: 100 μm.